

The REsonant Multi-Pulse Ionization injection

Paolo Tomassini¹, Sergio De Nicola², Luca Labate^{1,3}, Pasquale Londrillo⁴, Renato Fedele^{2,5}, Davide Terzani^{2,5} and Leonida A. Gizzi^{1,3}

¹*Intense Laser Irradiation Laboratory, INO-CNR, Pisa (Italy)**

²*Dip. Fisica Universita' di Napoli Federico II (Italy)*

³*INFN, Sect. of Pisa, (Italy)*

⁴*INAF, Bologna (Italy) and*

⁵*INFN, Sect. of Napoli (Italy)*

The production of high-quality electron bunches in Laser Wake Field Acceleration relies on the possibility to inject ultra-low emittance bunches in the plasma wave. In this paper we present a new bunch injection scheme in which electrons extracted by ionization are trapped by a large-amplitude plasma wave driven by a train of resonant ultrashort pulses. In the REsonant Multi-Pulse Ionization (REMPI) injection scheme, the main portion of a single ultrashort (e.g Ti:Sa) laser system pulse is temporally shaped as a sequence of resonant sub-pulses, while a minor portion acts as an ionizing pulse. Simulations show that high-quality electron bunches with normalized emittance as low as 0.08 mm×mrad and 0.65% energy spread can be obtained with a single present-day 100TW-class Ti:Sa laser system.

I. INTRODUCTION

High-quality Laser Wake Field Accelerated (LWFA) electron bunches are nowadays requested for several applications including Free Electron Lasers [1–3], X/γ radiation sources [4–8] and staged acceleration [9–13]. While performances of self-injected bunches generated in the so-called bubble-regime [14, 15] continue to improve, other promising injection schemes, including injection via density downramp [16–20], colliding pulses injection [21–23] and ionization injection [24–32], are under active theoretical and experimental investigation.

Evolutions of the ionization injection, based on the use of two laser pulses (either with the same or different wavelengths), were proposed in [33–36]. In the two-colour ionization injection [34] the main pulse that drives the plasma wave has a long wavelength, five or ten micrometers, and a large amplitude $a_0 = eA/mc^2 = 8.5 \cdot 10^{-10} \sqrt{I\lambda^2} > 1$, being I and λ pulse intensity in W/cm^2 and wavelength in μm . The second pulse (the “ionization pulse”) possesses a large electric field though its amplitude is low. This is achieved by doubling the fundamental frequency of a Ti:Sa pulse. While the main pulse cannot ionize the electrons in the external shells of the contaminant species due to its large wavelength, the electric field of the ionization pulse is large enough to generate newborn electrons that will be trapped in the bucket. This opens the possibility of using gas species with relatively low ionization potentials, thus enabling separation of wake excitation from particle extraction and trapping.

Two colour ionization injection is therefore a flexible and efficient scheme for high-quality electron bunch production. The main drawbacks of the two colour ionization injection are the current lack of availability of short ($T < 100$ fs) 100TW-class laser systems operating at large ($\approx 10\mu m$) wavelength and lasers synchronization jitter

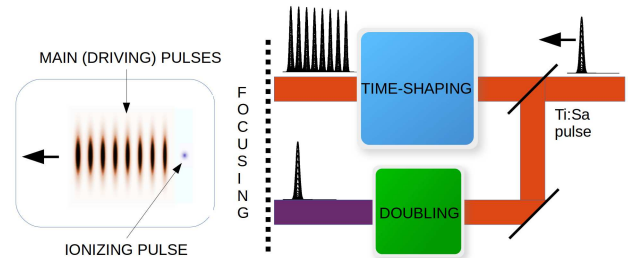


Figure 1. Multi-Pulse ionization injection scheme. A small fraction of a single Ti:Sa laser pulse is frequency doubled and will constitute the ionizing pulse. The main portion of the pulse is temporally shaped as a train of resonant pulses that will drive a large amplitude plasma wave.

issues. These limitations make the two-colour scheme currently unpractical for application to LWFA-based devices requiring high quality beams.

In this paper we propose a new injection configuration (we will refer to it as REsonant Multi-Pulse Ionization injection, REMPI) that overcomes these limitations and opens the way to a reliable generation of high quality Laser Wakefield accelerators. The breakthrough of our REMPI scheme is to replace the long wavelength driving pulse of the two-colour scheme with a short wavelength, resonant multi-pulse laser driver. Such a driver can be obtained via temporal shaping techniques from a *single*, linearly polarized, standard CPA laser pulse. A minor fraction of the same pulse is frequency doubled (or tripled) and used as ionizing pulse. Due to the resonant enhancement of the ponderomotive force, a properly tuned train of pulses is capable of driving amplitude waves larger than a single pulse with the same energy [37, 38] (see Fig. 2 where a comparison between a single-pulse and an eight-pulses train is shown). Noticeably, since the peak intensity of the driver is reduced by a fac-

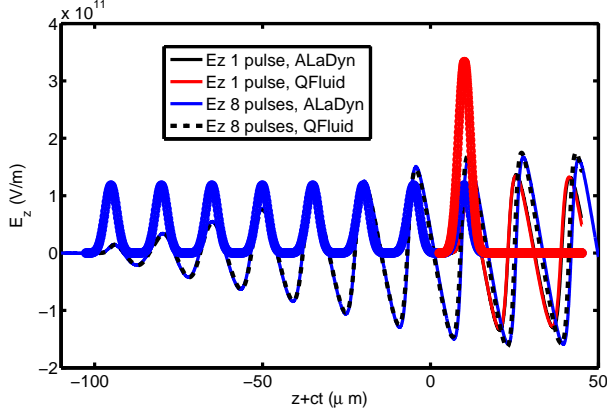


Figure 2. Single-pulse vs eight-pulses train comparison. Pulses (moving through the left) with duration of 10 fs and waist size of $25\ \mu\text{ m}$ are focused in a $n_e = 5 \times 10^{18}\text{ cm}^{-3}$ plasma. The single-pulse (red thick line) with peak intensity of $5.9 \times 10^{18}\text{ W/cm}^2$ drives a plasma wave whose maximum accelerating gradient is 20% less than that of the wave excited by the eight-pulses train having the same delivered energy and intensity $7.4 \times 10^{17}\text{ W/cm}^2$. QFluid and PIC (ALaDyn 2D) simulation are in excellent agreement.

tor equal to the number of train pulses, it is also possible to match the conditions of *both* particle trapping and unsaturated ionization of the active atoms level. Recently [39, 40] exciting experimental results on the generation of such a time shaped pulses demonstrate that a multi pulse scheme is obtainable with present day technology.

In Sec II we set-up trapping conditions for electrons extracted in a plasma wave driven by a resonant train of pulses. In Sec. III we will discuss in details the process of electron extraction by a linearly polarized ultraintense pulse. We carried on extensive numerical simulations to evaluate applicability and robustness of the scheme. Among them, in Sec. IV we will report on the simplest case of un-guided pulses designed for a state-of-the-art 250TW Ti:Sa laser system. Finally, Sec. VI is devoted to discussion of the results obtained by our simulations. In the Appendices details on the ADK ionization model will be found, along with a description of the hybrid fluid/kinetic QFluid code used for the simulations.

II. TRAPPING CONDITIONS IN REMPI

To set conditions of particles trapping in the plasma wave we will focus on a laser pulse configuration with a beam waist w_0 exceeding the plasma wavelength λ_p , where the longitudinal ponderomotive force dominates over radial wakefield force. In the 1D limit, the Hamiltonian of a passive particle in the plasma wave is [41] $H = (1 + u_z^2)^{1/2} - \beta_{ph}u_z - \phi$ where β_{ph} is wave phase velocity (transverse contribution to the Lorentz factor has been neglected since relatively low values of the pulse am-

plitudes will be considered here). The separatrix Hamiltonian H_s decomposes the phase space in a sequence of periodic buckets, so trapping of newborn electrons occurs if the particle Hamiltonian satisfies $H \leq H_s$, i.e if

$$\phi_e \geq 1 - 1/\gamma_{ph} + \phi_{min} \quad (1)$$

being ϕ_e the normalized electrostatic potential at particle extraction and ϕ_{min} the minimum potential. Eq. 1 clearly states that trapping condition relies on wave phase velocity and on wake electrostatic potential, i.e. on plasma density and normalized electric field $E_{norm} = E_z/E_0$ solely, being $E_0 = mc\omega_p/e$. Exact solution of the fully nonlinear wave equation in the 1D limit gives us a relationship between the normalized electric field and maximum/minimum potential [41] $\phi_{max,min} = E_{norm}^2/2 \pm \beta_{ph}\sqrt{(1 + E_{norm}^2/2)^2 - 1}$.

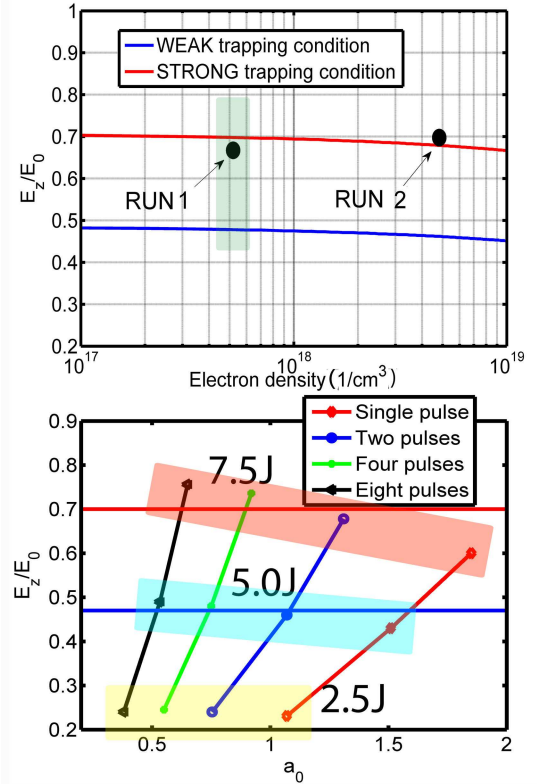


Figure 3. Trapping conditions. Blue lines: weak trapping threshold; red lines: strong trapping condition. Top: trapping conditions in a 1D nonlinear limit vs plasma density from 1D analytical expression Eq. 2 and 3. RUN 1,2 refer to the working points of the state-of-the-art simulation (Sec. IV) and the simulation in Appendix II, respectively. Bottom: scan of maximum accelerating normalized fields as in the RUN 1 setup ($T = 30\text{ fs}$, $n_e = 5 \times 10^{17}\text{ cm}^{-3}$, $w_0 = 45\ \mu\text{ m}$) as a function of pulse amplitude and the number of pulses in the train. The cases of a single pulse and two, four and eight-pulses trains with three different delivered energies of 2.5 J , 5.0 J and 7.5 J have been considered.

Trapping starts when Eq. 1 holds, i.e. when electrons reach the end of the bucket with the same speed as the wake phase speed ($v = \beta_{ph}c$). Since these electrons will not be accelerated further, we will refer to this condition as a “weak trapping condition”

$$2\beta_{ph}\sqrt{(1 + E_{norm}^2/2)^2 - 1} \geq 1 - 1/\gamma_{ph}. \quad (2)$$

Moreover, electrons that reach the speed of the wake before they experience the maximum accelerating field will dephase in the early stage of acceleration. As a consequence, a “strong trapping condition” can be introduced in such a way that electrons move with $v = \beta_{ph}c$ when they are in phase with the maximum longitudinal accelerating field. In this case the potential at $E_z = E_{max}$ is null, so we get

$$E_{norm}^2/2 + \beta_{ph}\sqrt{(1 + E_{norm}^2/2)^2 - 1} \geq 1 - 1/\gamma_{ph}. \quad (3)$$

Trapping analysis (see Fig. 3) reveals that efficient trapping occurs in a nonlinear wave regime since $E_{norm} > 0.5$, but well below longitudinal wavebreaking for a cold nonrelativistic plasma ($E_{norm} < 1$). Such an analysis is confirmed by our simulations and it is useful to set trapping threshold values for peak pulse amplitude a_0 in single or multi-pulse schemes.

If a plasma density of $n_e = 5 \times 10^{17} \text{cm}^{-3}$ is selected, a matched set of parameters gives a pulse duration of $T = 30$ fs FWHM, with a minimum waist $w_0 = 45 \mu\text{m}$ (the same parameters set will be used in the 250 TW state-of-the-art simulation, see below). A scan of the maximum accelerating field versus pulse amplitude and the number of pulses in the train is reported in Fig. 3. Three delivered energies of 2.5 J, 5.0 J and 7.5 J have been considered and, for any of them, a single-pulse, two, four and eight-pulses trains have been simulated. As shown in Fig. 3 (bottom), for a fixed total delivered laser energy, as the number of pulses in the train increases the maximum accelerating gradient of the wake increases due to a resonance enhancement of the wave. Moreover, from Fig. 3 (top and bottom) we can infer that the weak-trapping threshold Eq.2 is reached with a single-pulse of amplitude exceeding $a_0 = 1.6$, while in the case of a eight-pulses train, weak-trapping threshold amplitude is reduced to $a_0 = 0.5$.

III. IONIZATION DYNAMICS IN LINEAR POLARIZATION

Ultraintense laser pulses possess electric fields large enough to make tunneling as the dominant ionization mechanism (i.e. Keldysh parameter $\gamma_K = \sqrt{2U_I/mc^2}/a_0 \ll 1$) so as the Ammosov-Delone-Krainov (ADK) ionization rate [42] can be assumed to

evaluate electron extraction from the initial level (see Appendix). Ionization potential of 6th electron from Nitrogen is $U_I^{6th} = 552 \text{eV}$ and efficient extraction of 6th electron of Nitrogen requires $a_0 \approx 1.7$ for a few tens of femtoseconds long pulses at $\lambda = 0.8 \mu\text{m}$. On the other hand, Argon can be ionized from level 8th to level 9th ($U_I^{9th} = 422.5 \text{eV}$) at a much lower intensity, being $a_0 \approx 0.8$ and $a_0 \approx 0.4$ with $\lambda = 0.8 \mu\text{m}$ and $\lambda = 0.4 \mu\text{m}$, respectively.

We point out that a detailed description of ionization dynamics is crucial not only to correctly estimate the number of bunch electrons but (more importantly) to get a precise measure of the transverse phase space covered by newborn electrons. In the linear polarization case most of the electrons are ejected when the local electric field is maximum, i.e. when the pulse potential a_e is null. These electrons will leave the pulse with a negligible quivering mean momentum along the polarization axis x . If newborn electrons leave the atom when electric field is not exactly at its maximum, a non null transverse momentum $u_x = p_x/mc = -a_e$ is acquired, being a_e the local pulse potential at the extraction time. Moreover, ponderomotive forces introduce an axisymmetrical contribution to particles transverse momentum. Following [43] we can write an expression for the *rms* momentum along the x direction as a function of the pulse amplitude *envelope* at the extraction time a_{0e}

$$\sigma_{u_x} \cong \Delta \cdot a_{0e} = \sqrt{a_{0e}^3/a_c} \quad (4)$$

where $a_c = 0.107 (U_I/U_H)^{3/2} \lambda$ is a critical pulse amplitude and $\Delta = \sqrt{a_{0e}/a_c}$ (see Eqq. 7 and 10 in [43]). Eq. 4 gives us an accurate estimate of the minimum transverse momentum obtainable by the ionization process.

Trapping analysis with a standard *single* pulse shows that Nitrogen could be used in a simplified ionization injection (as suggested in [34]). Since efficient ionization threshold for N^{6+} is $a_0 \approx 1.7$ for $\lambda = 0.8 \mu\text{m}$, a small interval of $1.6 < a_0 < 1.7$ for the pulse amplitude is suitable for both trapping and ionization purposes. Such a simplified scheme could be useful either for demonstration purposes or to obtain a controlled injection for good-quality bunches without ultra-low emittance requirements. A two-pulses driver is a far better choice since an optimal pulse amplitude $1.1 < a_0 < 1.3$ allows us to strongly inhibit driver pulses ionization. Using Argon ($Ar^{8+} \rightarrow Ar^{9+}$) as a contaminant instead of Nitrogen gives us a drastic reduction of transverse particle momentum. Multi-pulse ionization injection with Argon requires trains with at least four pulses since ionization level is saturated with amplitude above $a_0 = 0.8$ at $\lambda = 0.8 \mu\text{m}$.

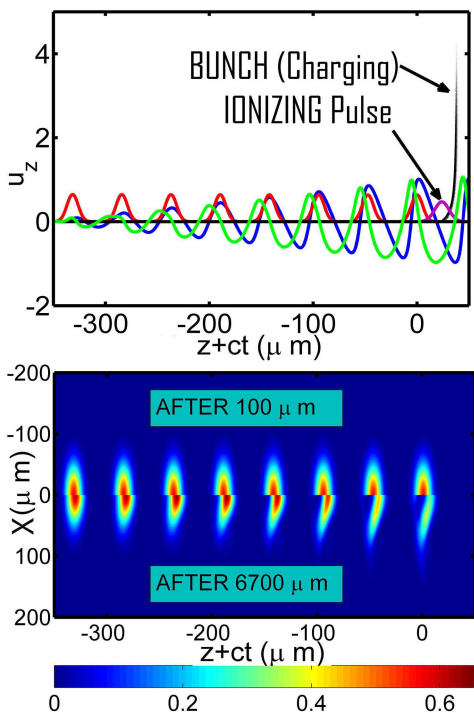


Figure 4. QFluid Snapshot after $100 \mu\text{m}$ of propagation and after 6.5 mm . Top: (after $100 \mu\text{m}$) lineout of the pulses amplitudes (red/purple lines), accelerating gradient (blue line) fluid longitudinal momentum (green line) and extracted particle's longitudinal phase-space. Electrons ejected by the driving pulse train don't comply with trapping conditions and move as a (quasi) fluid. Bottom: laser pulse amplitude comparison after $100 \mu\text{m}$ (upper) and after 6.5 mm (lower).

IV. STATE-OF-THE-ART 250 TW SIMULATION

The reported simulation (RUN 1) of our REsonant Multi-Pulse Ionization injection is based upon a linearly polarized Ti:Sa laser pulse that is initially split into the ionizing pulse and the eight-pulses driver train, each sub-pulse being 30 fs FWHM in duration and delivering 895 mJ of energy, with a maximum pulse amplitude $a_0 = 0.64$ and minimum waist size $w_0 = 45 \mu\text{m}$. The uniform plasma electron density is set to $n_e = 5 \times 10^{17} \text{ cm}^{-3}$ (plasma wavelength is $\lambda_p = 46.9 \mu\text{m}$), obtained with a pure Argon pre-ionized up to level 8^{th} . The frequency doubled component ($\lambda_{ion} = 0.4 \mu\text{m}$) with amplitude $a_{0,ion} = 0.41$ and duration $T_{ion} = 38 \text{ fs}$ is focused with a waist $w_{0,ion} = 3.5 \mu\text{m}$. The simulation (see Fig. 4) has been performed in a moving cylinder having a radius $4 \times w_0$ with a resolution of $\lambda_p/100$ and $\lambda_p/200$ in the radial and longitudinal coordinates, respectively.

Electrons extracted in the bulk of the ionizing pulse move suddenly backwards in the wake reaching the peak of the accelerating gradient of relative intensity $E_{norm} = E_z/E_0 = 0.685$, i.e. very close to the strong-trapping condition (see Fig. 3). Even though the driving pulse

sequence generates a marginal further ionization of Ar^{8+} with a maximum percentage ionization of about 3%, such a dark current will not be trapped in the wake (particles are extracted away from the optimal extraction point of maximum potential ϕ_{max}) and so it will have no detrimental effect on beam quality. Moreover, the short Rayleigh length $Z_R = \pi w_{0,ion}^2/\lambda_{ion} \approx 100 \mu\text{m}$ ensures a sudden truncation of beam charging that turns into a small rms absolute energy spread $\Delta E \approx E_{norm} \times E_0 \times Z_R \approx 5 \text{ MeV}$ and extracted charge $Q = 3.8 \text{ pC}$.

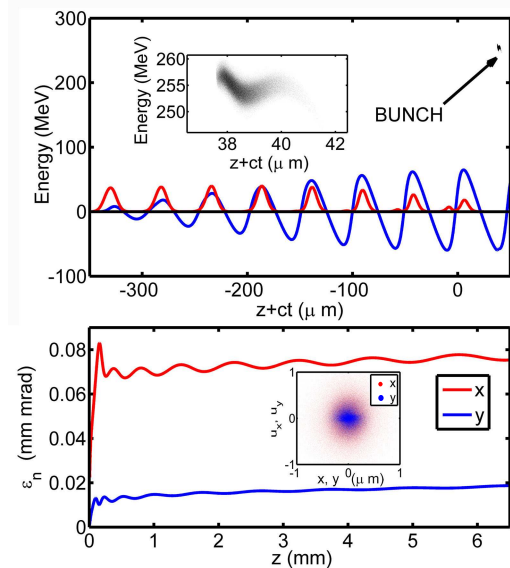


Figure 5. Bunch quality. Top: Final longitudinal position-energy distribution. Blue and red lines represent the accelerating gradient and pulse amplitude on axis on a.u., respectively. Inset: zoom of the longitudinal phase space. Bottom: Normalized emittance in $\text{mm} \times \text{mrad}$ as bunch moves into the wake. Inset: final transverse phase space.

At the end of beam charging, i.e after about $200 \mu\text{m}$ of propagation, the *rms* bunch length is $0.56 \mu\text{m}$ and the transverse normalized emittance is $\epsilon_{n,x} = 0.070 \text{ mm} \times \text{mrad}$ in the polarization direction x and $\epsilon_{n,y} = 0.016 \text{ mm} \times \text{mrad}$ along the y direction. Afterwards, the *quasi-matched* beam experiences dumped betatron oscillations with converging beam radius of $0.4 \mu\text{m}$ that generate an emittance growth of about 10% as simulation ends (see Fig. 5).

Since in the weak nonlinear regime there's no electron density cavitation as in the bubble regime, beam loading might be a serious limit for beam quality. In the current working point, however, beam loading is present but exerts a tiny perturbation (of about 1%) of the longitudinal field on the bunch core, as it is apparent in Fig. 6. We expect, therefore, that the transverse asymmetry of the bunch ($\sigma(x) \approx 2\sigma(y)$) arising from the initial transverse momentum will generate asymmetric beam loading effects but with very low amplitude.

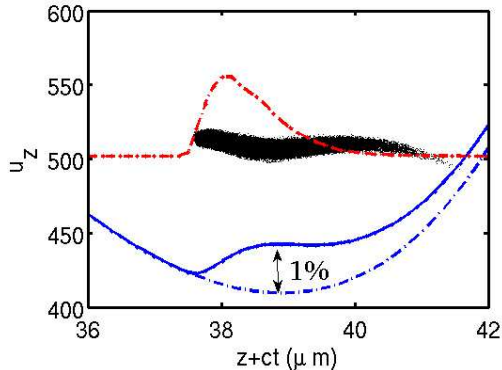


Figure 6. Beam loading effect at the end of the simulation. The longitudinal phase space of the beam is shown along with the (on axis) beam density (red line), accelerating field (full blue line) and reference field without beam-loading (dashed blue line). Beam loading makes a decrease of the longitudinal field of about 1% at most.

At the end of the 6.5 mm long extraction/acceleration phase the bunch has mean energy 265 MeV, with final normalized emittances of 0.076 mm×mrad (x axis) and 0.018 mm×mrad (y axis), with an *rms* energy spread 0.65% and peak current of about 1 kA. These extremely low values of emittance and energy spread show that the proposed REsonant Multi-Pulse Ionization injection scheme is ideal for the generation of very high quality accelerated bunches.

V. CONCLUSIONS

We propose a new ultra-low emittance LWFA injector scheme that uses a Resonant train of pulses to drive plasma waves having amplitude large enough to trap and accelerate electrons extracted by ionization. The pulses train is obtained by temporal shaping of an ultrashort pulse. Unlike two-colour ionization injection, a single laser system (e.g Ti:Sa) can be therefore employed to both drive the plasma wave and extract newborn electrons by ionization. Simulations consistently show that the main processes, including extraction of electrons due to the ionizing pulse, their trapping in the bucket and subsequent acceleration can be controlled by tuning electron density and laser intensity. Simulations also show a negligible contribution of spurious electrons extracted directly by the driver pulses. Simulations carried out in different plasma conditions show feasibility of the scheme with state-of-the-art-lasers making REMPI suitable either for direct interaction (e.g Thomson Scattering or FEL) or as ultra-low emittance injector for GeV-scale energy boosting.

Very recently J. Cowley et al. [40] reported on very encouraging results about the feasibility of their time-shaping setup, with the demonstration of efficient exci-

tation of the plasma wave via Multi-Pulse LWFA. The REMPI scheme could be tested with two pulses in the train at first, with Nitrogen as a contaminant species. In order to obtain very good-quality electron bunches, however, Argon should be preferred and in this case more than four pulses in the train are necessary as shown in Sec. II.

VI. ACKNOWLEDGMENTS

The research leading to these results has received funding from the European Union's Horizon 2020 research and innovation programme under Grant Agreement No 653782 - EuPRAXIA. Authors wish to thank CNAF-INFN for access to computational resources. Authors also acknowledge support from Manuel Kirchen from Hamburg University for his help about the FB-PIC code.

VII. APPENDIX I. ADK IONIZATION RATE

In this paper we use the following formulation of the instantaneous ADK ionization rate in the tunnelling regime [42]

$$w_{ADK}(|m|) = C \times \rho_{ADK}^{n(|m|)} \times \exp(-1/\rho_{ADK}), \quad (5)$$

where $n(|m|) = -2n^* + |m| + 1$, C is a coefficient depending on the atomic numbers and ionization energy U_I ($U_H = 13.6eV$)

$$C = \frac{1}{4\pi} \left(\frac{U_I}{U_H} \right)^{3/2} 3^{(2n^* - |m| - 1)} \left[\frac{4e^2}{n^{*2} - l^{*2}} \right]^{n^*} \left[\frac{n^* - l^*}{n^* + l^*} \right]^{l^* + \frac{1}{2}}, \quad (6)$$

and $\rho_{ADK} = 3/2 (E/E_{at}) (U_H/U_I)^{3/2}$, being $E_{at} = 0.514 TV/m$ and E the atomic and the local electric fields, respectively. The effective quantum numbers are $n^* = Z\sqrt{U_H/U_I}$ and $l^* = n_0^* - 1$, being n_0^* referred to the lower state with the same l . A critical electric field $E_c = 2/3 E_{at} (U_I/U_H)^{3/2}$, giving a scale of a short-time scale ionization, can be introduced. By expressing E/E_c using vector potentials we get $a/a_c = \rho_{ADK} = 9.37 (U_H/U_I)^{3/2} a/\lambda$ which is nothing but the square of Δ parameter in [43].

In the circularly polarized pulse case the electric field rotates within each cycle still retaining the same intensity, so in the tunnelling regime the mean-cycled ionization rate coincides with the instantaneous rate of Eq. 5

$$\langle w_c \rangle = w_{ADK}. \quad (7)$$

In the linearly polarized pulse case the mean over a cycle can be performed analytically after a Taylor expansion

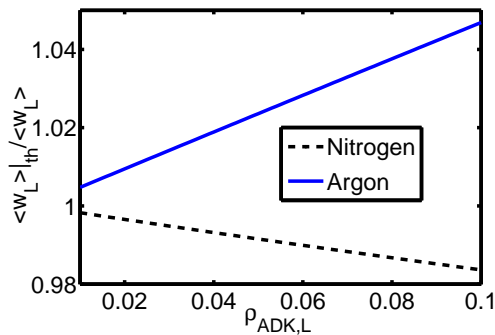


Figure 7. Comparison between the numerical estimation of the mean-cycled ADK rate and the widely used analytical result of Eq. 9 for Ar^{9+} and N^{6+} final states.

of the leading exponential term. The well known result (rewritten in our notation) is

$$\langle w_L \rangle = w_{ADK}(\rho_{ADK,0}) \times \left(\frac{2}{\pi} \rho_{ADK,0}\right)^{1/2}, \quad (8)$$

where $\rho_{ADK,0}$ is the peak value of $\rho_{ADK} = a/a_c$ within the cycle. A numerical estimation of the mean-cycled rate confirms the validity of Eq. 8 with errors below 4% in the ionization rates, for ρ_{ADK} parameters in the range of interest for ionization injection techniques (see Fig. 7).

VIII. APPENDIX II QFLUID CODE

QFluid is a cold-fluid/kinetic code in 2D *cylindrical* coordinates, employing plasma dynamics in a Quasi Static Approximation [46]. Electrons macroparticles move kinetically in a full 3D dynamics depicted by the longitudinal E_z and radial E_r electric field, the azimuthal magnetic field B_ϕ and ponderomotive forces due to laser pulses. The main laser pulse train propagates following the envelope evolution equation with the second time derivative included [47], while the evolution of the ionization pulse follows the Gaussian pulse evolution prescription. For our purposes, in the absence of non-fluid plasma behavior, strong longitudinal background gradients and radial anisotropies, QFluid returns the same results of a 3D PIC code with much less demanding computation time/resources. Particle extraction from atoms/ions is simulated with an ADK rate including the mean over a pulse cycle, while newborn particles are finally ejected with a random transverse momentum u_\perp , whose rms value depends on the polarization of the pulses. For a linear polarization (as for the ionizing pulse) we assigned $\sigma_{u_x} \cong \Delta \cdot a_{0e} = \sqrt{a_{0e}^3/a_c}$ (see Eq. 4), while for the circular polarization each extracted particle is associated to a random extraction phase ϕ_e so as $u_x = a_{0e} \times \cos(\phi_e)$, $u_y = a_{0e} \times \sin(\phi_e)$. Benchmark of QFluid with a multi-pulse setup has been obtained in a nonlinear regime with

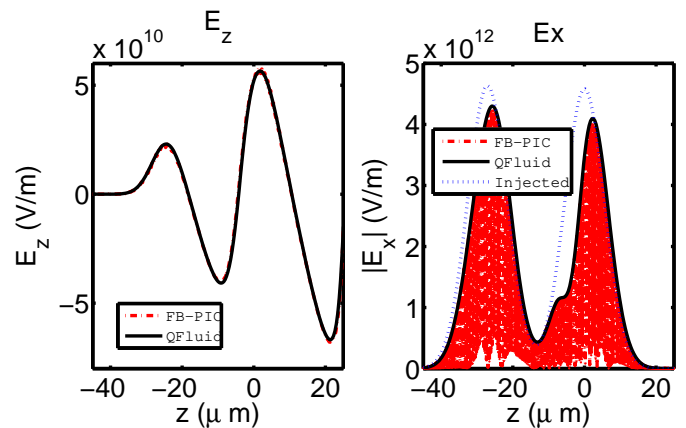


Figure 8. FB-PIC vs QFluid in a two-pulses driver configuration with Nitrogen. Snapshot after $700 \mu m$ of propagation into a plasma with background density of $n_e = 1.5 \times 10^{18} cm^{-3}$. Left: longitudinal electric field on axis. Right: pulse electric field (FB-PIC) and its amplitude (QFluid). The injected pulse amplitude (blue dotted line) has been shown for reference.

ALaDyn [44] (used here in either a 3D with laser envelope configuration or a 2D slice with a full-PIC pulse evolution) and with FB-PIC (quasi-3D PIC) [49].

The comparison of QFluid with FB-PIC is focused on a 2-pulses driver scheme with Nitrogen as atomic species. The selected working point consists of linearly polarized pulses of duration $T = 30 fs$, minimum waist size $w_0 = 12 \mu m$ and amplitude $a_0 = 1.2$ delayed by a plasma wavelength ($\lambda_p = 27 \mu m$ with $n_e = 1.5 \times 10^{18} cm^{-3}$). FB-PIC simulations were performed with two azimuthal modes, i.e. possible deviation from perfect azimuthal symmetry were included.

The comparison between FB-PIC and QFluid simulation (see Fig. 8) shows a perfect superposition between the codes output, notwithstanding the nontrivial evolution of the pulses due to both nonlinear effects and the variation of the susceptibility due to the wake.

The first QFluid and ALaDyn comparison shown here, has been focused on an eight-pulses drivers train with Argon as atomic species, with selected working point as the same as the state-of-the-art setup. To fasten the 3D PIC simulation, ALaDyn has been equipped with an envelope pulse solver. The Aladyn/envelope code implements a fully 3D PIC scheme for particle motion whereas the laser pulses are represented by the envelope model proposed in [50].

Once again (see Fig. 9), QFluid outcomes deviate at most of a few percent from those of a 3D PIC (full 3D in this case).

Finally, a full-PIC (not in envelope approximation) in 2D slice geometry *vs* QFluid comparison, including the bunch extraction and trapping, will be presented (RUN 2). To save computational time an high-density setup has been simulated. A train of eight $10 fs$ linearly po-

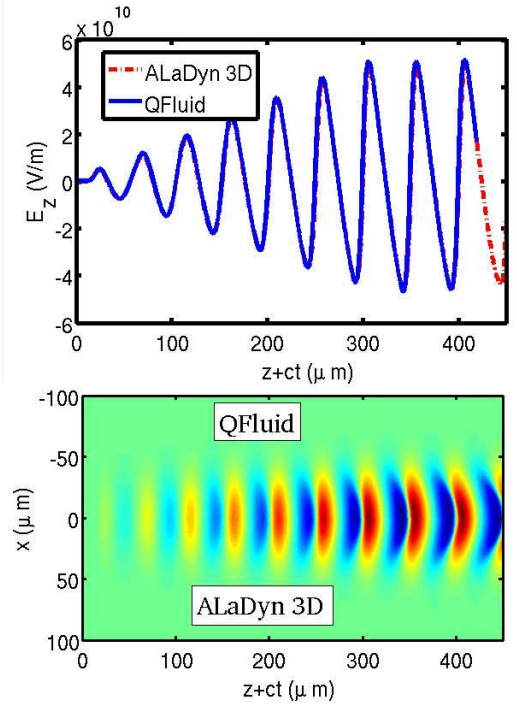


Figure 9. ALaDyn vs QFluid in a eight-pulses setup with Argon (state-of-the-art run parameters). Top: Snapshot of the on-axis longitudinal electric field after 1 mm of propagation. Bottom: radial maps of $E_{norm} = E_z/E_0$ for Qfluid (upper side) vs ALaDyn (lower side).

larized Ti:Sa pulses impinge onto a preformed plasma of Ar^{8+} with density $5 \times 10^{18} \text{cm}^{-3}$. The driver pulse train has a waist size $w_0 = 25 \mu\text{m}$ and an amplitude $a_0 = 0.589$, having a pulse delay of a single plasma period $T_p = 2\pi/\omega_p$. We use a relatively large focal spot with $w_0 > \lambda_p = 14.8 \mu\text{m}$, so as to reduce the effects of the missing third dimension in the PIC simulations. The frequency doubled ionizing pulse is injected with a delay of $1.5 \times T_p$ in the vicinity of its focus with a waist $w_{0,inj} = 3.5 \mu\text{m}$ and possesses a peak pulse amplitude of $a_{0,inj} = 0.41$. PIC simulations were performed with a $170 \times 150 \mu\text{m}^2$ box in the longitudinal and transverse directions with a resolution of $\lambda/40$ and $\lambda/10$, respectively. QFluid simulations were carried out in the same (cylindrical) box size with resolution $\lambda_p/70$ and $\lambda_p/35$ in the longitudinal and radial coordinates, respectively.

The final snapshot of both simulation, after 300 μm propagation in the plasma is shown in Fig. 10, where the injected electron bunch just at the end of the charging phase is visible (black and blue dots). Due to the large ponderomotive forces (that scale as $a_{0,inj}^2/w_{0,inj}$, see Eq. 23 in [43]), bunch transverse *rms* momentum (0.26 mc for QFluid and 0.27 mc for ALaDyn, respectively) shows an increase of about a factor of 2 from the value expected by Eq. 4.

We finally stress that QFluid cannot face with the

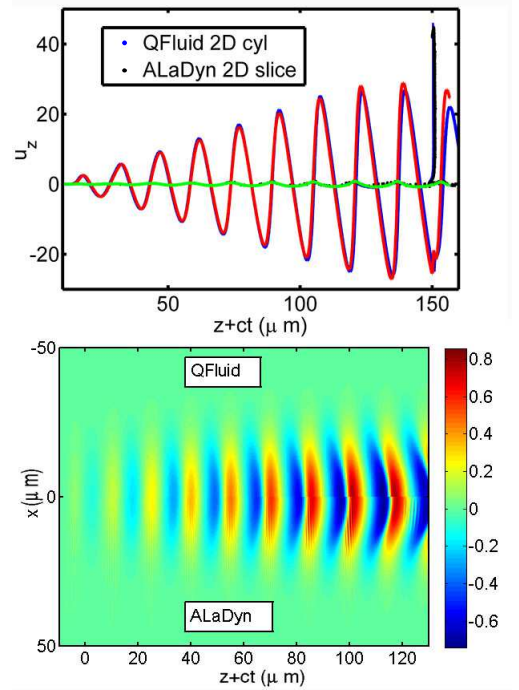


Figure 10. 2D-slice ALaDyn and QFluid in RUN 2 setup. QFluid and ALaDyn PIC results after 300 μm of propagation. Top: (on-axis) ALaDyn phase space of particles (black dots), QFluid phase space of particles (blue dots), ALaDyn accelerating field (blue line, a.u.) and QFluid accelerating field (red line, a.u.). The green line represents fluid momentum of QFluid output. Bottom: Longitudinal electric field $E_{norm} = E_z/E_0$ from QFluid (upper) and ALaDyn (lower).

plasma exit of the generated bunch since the Quasi Static Approximation requires a steady plasma density within the box. A PIC code will be used in a future work to simulate the plasma exit, too.

* paolo.tomassini@ino.it

- [1] K. Nakajima, Few femtosecond, few kiloampere electron bunch produced by a laser-plasma accelerator; *Nature Physics* 4, 92 - 93 (2008).
- [2] V. Petrillo, M. P. Anania, M. Artioli, A. Bacci, M. Bellaveglia, E. Chiadroni, A. Cianchi, F. Ciocci, G. Dattoli, D. Di Giovenale, G. Di Pirro, M. Ferrario, G. Gatti, L. Giannessi, A. Mostacci, P. Musumeci, A. Petralia, R. Pompili, M. Quattromini, J. V. Rau, C. Ronsivalle, A. R. Rossi, E. Sabia, C. Vaccarezza, and F. Villa, Observation of Time-Domain Modulation of Free-Electron-Laser Pulses by Multiplexed Electron-Energy Spectrum; *Phys. Rev. Lett.* 111, 114802 (2013).
- [3] A. Loulergue, M. Labat, C. Evain, C. Benabderrahmane, V. Malka and M. E. Couprie, Beam manipulation for compact laser wakefield accelerator based free-electron lasers, *New J. Phys.* 17, 023028 (2015).
- [4] E. Esarey, S. K. Ride, and P. Sprangle, Nonlinear Thomson scattering of intense laser pulses from beams and

- plasmas, *Phys. Rev. E* 48, 3003 (1993).
- [5] P. Tomassini, A. Giulietti D. Giulietti and L. A. Gizzi, Thomson backscattering X-rays from ultra-relativistic electron bunches and temporally shaped laser pulses, *Appl Phys. B* 80, 4, pp 419–436 (2005).
- [6] S. Corde, K. Ta Phuoc, G. Lambert, R. Fitour, V. Malka, A. Rousse, A. Beck, and E. Lefebvre, Femtosecond x rays from laser-plasma accelerators, *Rev. Mod. Phys.* 85, 1 (2013);
- [7] V. Petrillo, A. Bacci, C. Curatolo, I. Drebot, A. Giribono, C. Maroli, A. R. Rossi, L. Serafini, P. Tomassini, C. Vaccarezza, and A. Variola, Polarization of x-gamma radiation produced by a Thomson and Compton inverse scattering, *Phys. Rev. ST-AB* 18, 110701 (2015);
- [8] D. Micieli, I. Drebot, A. Bacci, E. Milotti, V. Petrillo, M. Rossetti Conti, A. R. Rossi, E. Tassi, and L. Serafini, Compton sources for the observation of elastic photon-photon scattering events, *Phys. Rev. ST-AB* 19, 093401 (2016).
- [9] A. Döpp, E. Guillaume, C. Thaurya), A. Lifschitz, K. Ta Phuoc, and V. Malka, Energy boost in laser wakefield accelerators using sharp density transitions, *Phys. Plasmas* 23 (5), 056702 (2015).
- [10] S. Steinke , , J. van Tilborg , C. Benedetti , C. G. R. Geddes , J. Daniels , K. K. Swanson , A. J. Gonsalves , K. Nakamura , B. H. Shaw , C. B. Schroeder , E. Esarey , and W. P. Leemans, Staging of laser-plasma accelerators, *Physics of Plasmas* 23 , 056705 (2016); doi: 10.1063/1.494828
- [11] T.L. Audet, F.G. Desforages, A. Maitrallain, S. Dobosz Dufrénoy, M. Bougeard, G. Maynard, P. Lee, M. Hansson, B. Aurand, A. Persson, I. Gallardo González, P. Monot, C.-G. Wahlström, O. Lundh, B. Cros, Electron injector for compact staged high energy accelerator, *NIM A* 829, 304-308 (2016).
- [12] G. Golovin, S. Banerjee, S. Chen, N. Powers , C. Liu, W. Yan, J. Zhang, P. Zhang, B. Zhao, D. Umstadter, Control and optimization of a staged laser-wake field accelerator, *NIM A* 830, 375-380 (2016).
- [13] Zhijun Zhang, Wentao Li, Jiansheng Liu , Wentao Wang, Changhai Yu, Ye Tian, Kazuhisa Nakajima, Aihua , , Deng, Rong Qi, Cheng Wang, Zhiyong Qin, Ming Fang, Jiaqi Liu, Changquan Xia, Ruxin Li , and Zhizhan Xu, Energy spread minimization in a cascaded laser wakefield accelerator via velocity bunching, *Physics of Plasmas* 23, 053106 (2016); doi: 10.1063/1.4947536
- [14] J. Faure, Y. Glinec, A. Pukhov, S. Kiselev, S. Gordienko, E. Lefebvre, J.-P. Rousseau, F. Burgy, V. Malka, A laser-plasma accelerator producing monoenergetic electron beams, *Nature* 541, 431(2004).
- [15] G. R. Plateau, C. G. R. Geddes, D. B. Thorn, M. Chen, C. Benedetti, E. Esarey, A. J. Gonsalves, N. H. Matlis, K. Nakamura, C. B. Schroeder, S. Shiraishi, T. Sokollik, J. van Tilborg, Cs. Toth, S. Trotsenko, T. S. Kim, M. Battaglia, Th. Stöhlker, and W. P. Leemans, Low-Emittance Electron Bunches from a Laser-Plasma Accelerator Measured using Single-Shot X-Ray Spectroscopy, *Phys. Rev. Lett.* 109, 064802 (2012).
- [16] S. Bulanov, N. Naumova, F. Pegoraro, and J. Sakai, Particle injection into the wave acceleration phase due to nonlinear wake wave breaking, *Phys. Rev. E* 58 , R5257 (1998).
- [17] H. Suk, N. Barov, J.B. Rosenzweig and E. Esarey, Plasma Electron Trapping and Acceleration in a Plasma Wake Field Using a Density Transition, *Phys. Rev. Lett.* 86, 1011-1014 (2001).
- [18] P. Tomassini, M. Galimberti, A. Giulietti, D. Giulietti, L. A. Gizzi, L. Labate, and F. Pegoraro, Production of high-quality electron beams in numerical experiments of laser wakefield acceleration with longitudinal wave breaking, *Phys. Rev. ST Accel. Beams* 6 , 121301 (2003).
- [19] C. G. R. Geddes, E. Cormier-Michel, E. Esarey, K. Nakamura, G. R. Plateau, C. B. Schroeder, Cs. Toth, D. L. Bruhwiler, J. R. Cary, and W. P. Leemans, Plasma gradient controlled injection and postacceleration of high quality electron bunches, *Proceedings of the Thirteenth Advanced Accelerator Concepts Workshop*, 1086 (2008).
- [20] A. Buck, J. Wenz, J. Xu, K. Khrennikov, K. Schmid, M. Heigoldt, J. M. Mikhailova, M. Geissler, B. Shen, F. Krausz, S. Karsch, and L. Veisz, Shock-Front Injector for High-Quality Laser-Plasma Acceleration, *Phys. Rev. Lett.* 110, 185006 (2013).
- [21] E. Esarey, R. F. Hubbard, W. P. Leemans, A. Ting, and P. Sprangle, Electron Injection into Plasma Wakefields by Colliding Laser Pulses, *Phys. Rev. Lett.* 79, 2682 (1997).
- [22] H. Kotaki, *et al.* , Electron Optical Injection with Head-On and Countercrossing Colliding Laser Pulses, *Phys. Rev. Lett.* 103, 194803 (2009).
- [23] M. Chen, E. Esarey, C. G. R. Geddes, E. Cormier-Michel, C. B. Schroeder, S. S. Bulanov, C. Benedetti, L. L. Yu, S. Rykovanov, D. L. Bruhwiler, and W. P. Leemans, Electron injection and emittance control by transverse colliding pulses in a laser-plasma accelerator, *Phys. Rev. ST Accel. Beams* 17, 051303 (2014).
- [24] Min Chen, Zheng-Ming Sheng, Yan-Yun Ma, and Jie Zhang, Electron injection and trapping in a laser wakefield by field ionization to high-charge states of gases, *Jour. Appl. Phys.* 99, 056109 (2006).
- [25] A. Pak, K. A. Marsh, S. F. Martins, W. Lu, W. B. Mori, and C. Joshi, Injection and Trapping of Tunnel-Ionized Electrons into Laser-Produced Wakes, *PRL* 104, 025003 (2010).
- [26] C. McGuffey *et al.* , Ionization induced trapping in a laser wakefield accelerator, *Phys. Rev. Lett.* 104, 025004 (2010).
- [27] C. Thaury, E. Guillaume, A. Lifschitz, K. Ta Phuoc, M. Hansson, G. Grittani, J. Gautier, J.-P. Goddet, A. Tafzi, O. Lundh & V. Malka, Shock assisted ionization injection in laser-plasma accelerators, *Scientific Reports* 5, 16310 (2015).
- [28] C. E. Clayton, J. E. Ralph, F. Albert, R. A. Fonseca, S. H. Glenzer, C. Joshi, W. Lu, K. A. Marsh, S. F. Martins, W. B. Mori, A. Pak, F. S. Tsung, B. B. Pollock, J. S. Ross, L. O. Silva, and D. H. Froula, Self-Guided Laser Wakefield Acceleration beyond 1 GeV Using Ionization-Induced Injection, *Phys. Rev. Lett.* 105, 105003 (2010).
- [29] M. Chen, E. Esarey, C. B. Schroeder, C. G. R. Geddes, and W. P. Leemans, Theory of ionization-induced trapping in laser-plasma accelerators, *Phys. Plasmas* 19, 033101 (2012).
- [30] M. Zeng, M. Chen, L. L. Yu, W. B. Mori, Z. M. Sheng, B. Hidding, D. A. Jaroszynski, and J. Zhang, Multichromatic Narrow-Energy-Spread Electron Bunches from Laser-Wakefield Acceleration with Dual-Color Lasers, *Phys. Rev. Lett.* 114, 084801 (2015).
- [31] Ming Zeng , Ji Luo, Min Chen, Warren B. Mori, Zheng-Ming Sheng, and Bernhard Hidding, High quality electron beam acceleration by ionization injection in laser

- wakefields with mid-infrared dual-color lasers, *Physics of Plasmas* 23, 063113 (2016); doi: 10.1063/1.4953895
- [32] T. L. Audet, M. Hansson, P. Lee, F. G. Desforges, G. Maynard, S. Dobosz Dufrenoy, R. Lehe, J.-L. Vay, B. Aurand, A. Persson, I. Gallardo González, A. Maitrallain, P. Monot, C.-G. Wahlström, O. Lundh, and B. Cros, Investigation of ionization-induced electron injection in a wakefield driven by laser inside a gas cell, *Physics of Plasmas* 23 023110 (2016).
- [33] N. Bourgeois, J. Cowley, and S. M. Hooker, Two-Pulse Ionization Injection into Quasilinear Laser Wakefields, *PRL* 111, 155004 (2013).
- [34] L.-L. Yu, E. Esarey, C. B. Schroeder, J.-L. Vay, C. Benedetti, C. G. R. Geddes, M. Chen, and W. P. Leemans, Two-Color Laser-Ionization Injection, *Phys. Rev. Lett.* 112, 125001 (2014).
- [35] L.-L. Yu, E. Esarey, C. B. Schroeder, J.-L. Vay, C. Benedetti, C. G. R. Geddes, M. Chen, and W. P. Leemans, Ultra-low emittance electron beams from two-color laser-ionization injection, *Advanced Accelerator Concepts 2014 AIP Conf. Proc.* 1777, 040019-1-040019-5; doi: 10.1063/1.4965621.
- [36] X.L. Xu et al, Low emittance electron beam generation from a laser wakefield accelerator using two laser pulses with different wavelengths, *Phys. Rev. ST Accel.Beams* 17 061301 (2014)
- [37] D. Umstadter, E. Esarey, and J. Kim, Nonlinear Plasma Waves Driven by Optimized Laser Pulse Trains, *Phys. Rev. Lett.* 72, 1224 (1994).
- [38] S M Hooker, R Bartolini, S P D Mangles, A Tunnermann, L Corner, J Limpert, A Seryi and R Walczak, Multi-pulse laser wakefield acceleration: a new route to efficient, high-repetition-rate plasma accelerators and high flux radiation sources, *J. Phys. B* 47, 234003 (2014).
- [39] R.J. Shalloo, L. Corner, C. Arran, J. Cowley, G. Cheung, C. Thornton, R. Walczak, S.M. Hooker, Generation of laser pulse trains for tests of multi-pulse laser wakefield acceleration, *NIM A* 829, 1, 383-385 (2016).
- [40] J. Cowley, C. Thornton, C. Arran, R. J. Shalloo, L. Corner, G. Cheung, C.D. Gregory, S.P.D. Mangles, N.H. Matlis, D.R. Symes, R. Walczak, and S. M. Hooker, Excitation and Control of Plasma Wakefields by Multiple Laser Pulse, *Phys. Rev. Lett.* 119, 044802 (2017).
- [41] E. Esarey and M. Pilloff, Trapping and acceleration in nonlinear plasma waves, *Phys. Plasmas* 2, 1432 (1995).
- [42] V.P. Krainov, W. Xiong, S.L. Chin, An introductory overview of tunnel ionization of atoms by intense lasers, *Laser Physics* 2, 4 (1992).
- [43] C. B. Schroeder, J.-L. Vay, E. Esarey, S. Bulanov, C. Benedetti, L.-L. Yu, M. Chen, C. G. R. Geddes, and W. P. Leemans, Thermal emittance from ionization-induced trapping in plasma accelerators, *Phys. Rev. ST AB* 17, 101301 (2014).
- [44] C. Benedetti, A. Sgattoni, G. Turchetti and P. Londrillo, ALaDyn: A High-Accuracy PIC Code for the Maxwell-Vlasov Equations, *IEEE Trans. On Pl. Science* 36, 4 (2008). Available at <https://github.com/ALaDyn/ALaDyn>
- [45] P. Tomassini and A.R. Rossi, Matching strategies for a plasma booster, *Plasma Phys. Control. Fusion* 58 034001 (2016);
- [46] P. Sprangle, E. Esarey and A. Ting, Nonlinear Theory of Intense Laser-Plasma Interaction, *Phys. Rev. Lett* 64, 2011-2014 (1990).
- [47] P. Sprangle, E. Esarey, and J. Krall, Self-guiding and stability of intense optical beams in gases undergoing ionization, *Phys. Rev. E* 54, 4211 (1996).
- [48] Ji-Wei Geng, L. Qin, Min Li, Wei-Hao Xiong, Y. Liu, Q. Gong and L-Y. Peng, Nonadiabatic tunneling ionization of atoms in elliptically polarized laser fields, *J. Phys. B: At. Mol. Opt. Phys.* 47 204027 (2014) .
- [49] R.Lehe, M. Kirchen, I. A. Andriyash, B. B. Godfrey, Jean-Luc Vay, A spectral, quasi-cylindrical and dispersion-free Particle-In-Cell algorithm, *Computer Physics Communications* 203, 66-82 (2015). Available at <http://fbpic.github.io>
- [50] P. Mora and T. M. Antonsen, Jr., Kinetic modeling of intense, short laser pulses propagating in tenuous plasmas, *Physics of Plasmas* 4, 217 (1997).